Indian Journal of Pure & Applied Physics
Vol. 62, July 2024, pp. 533-537
DOI: 10.56042/ijpap.v62i7.10033

The Advances in Structural, Optical and Magnetic Behaviour with Alumina Dopant's in $Fe_2Al_2O_{6-\delta}$ Nano-crystalline Structure

Seema[a*], Meenakshi[b], Praveen Bhatt[b], Rajesh Sharma[c] & Jyoti Dalal[d]

[a]Department of Physics, Research Scholar, Baba Mastnath University, Rohtak 124 021, India
[b]Department of Physics, Faculty of Sciences, Baba Mastnath University, Rohtak 124 021, India
[c]Department of Physics, Faculty of Sciences, M.N.S Govt. College, Bhiwani 127 021, India
[d]Department of Physics, Faculty of Sciences, Pt. N.R.S Govt. College, Rohtak 124 001, India

Received 31 March 2024; accepted 24 May 2024

In this present work, Fe_2O_3 nanoparticles doped with different concentrations of aluminium oxide (Al_2O_3) (5%, 10%, and 20%) were synthesized by the modified co-precipitation method, and samples were calcined at 600 ^oC for a fixed duration 2 hours. The calcined samples were examined through X-ray diffraction (XRD) techniques and results reveal that rhombohedral crystalline structures were confirmed for all calcined samples and the crystallite size of the particle increased from 42.2 nm to 60.5 nm i.e. crystallite size increases with increase of in dopant concentration alumina in $Fe_2Al_2O_{6-\delta}$ samples. The infrared spectroscopic results reveal that, as usual, peaks of hydroxyl group vibrations were found in band formation at about 3000 cm^{-1}, 1650 cm^{-1} and the sharp peaks at 610, 614, and 617 cm^{-1} were attributed to O-Fe-O molecules vibrations whereas, 533 cm^{-1} were attributed by O-Al-O molecules vibrations. The optical band gap was calculated via tauc plot and calculated values show an inverse trend of 2.19 to 2.15 eV with an increase in dopant concentration alumina. Vibrating sample magnetometer (VSM) were used to analyze the magnetic characteristics of calcined samples and the results reveal that saturation magnetization is highest for dopant alumina 10% concentration ($M_s = 50.6\times10^{-2}$ emu/g) and coercivity is highest for dopant alumina 5% concentration ($H_c = 875.38O_e$) respectively among all the calcined samples.

Keywords: Al_2O_3-doped; Fe_2O_3 nanoparticles; XRD; FTIR; UV-Vis; Structural; Optical and Magnetic properties

1 Introduction

Nanoparticle sizes usually range between 1-100 nm. The metallic nanoparticles differ from bulk metals in compare to their physical and chemical characteristics, especially changes were noticed in higher specific surface areas, mechanical strengths, specific optical qualities, lower melting points, and specific magnetization[1]. These differences could make metallic nanoparticles desirable for various industrial uses, *e.g.* Hyperthermia treatment, transparent sunscreens & scratch-proof eye-glasses, anti-graffiti coatings for walls, stain-repellent fabrics, and ceramic coatings for solar cells. On the other hand, specific applications greatly influence the idea and understanding of nanoparticles[2]. In nature, iron can be found as hydroxides, oxy-hydroxides, oxides, colloids and other molecular complexes. Furthermore, iron is also an essential element in some biological proteins like haemoglobin, myoglobin, ferritin, and transferrinetc. It is extensively used as catalysts, magnetic materials, colour pigments, and metallurgy based industrial uses[3,4]. In labs, the iron oxides are easily synthesized and found in various crystalline forms, i.e. in Haematite, Magnetite and Maghemite *etc*[5].Moreover, aluminium is the third most abundant metal in the lithosphere and the most common element in the earth's crust (~8%). Besides, aluminium is an active amphoteric metal that, under normal conditions, develops a white oxide film on its surface. Aluminium oxide's α-, β- and γ- phase changes are the most well-known and the most prevalent modification in nature is the α-modification of aluminium oxide (α-Al_2O_3), also called alumina[6]. Alumina nanoparticles possess a spherical shape due to its unique properties, it finds extensive use in a variety of consumable items, and cosmetic applications. With its high mechanical strength, large surface area compared to volume, high firmness, and good chemical stability, nano-sizedaluminium oxide (α-and γ-Al_2O_3) has found growing application in many different industries[7-9]. Similar to numerous other metal oxides, α-Fe_2O_3andAl_2O_3 can be synthesized by a range of methods, including the hydrothermal method, sol-gel, thermal

*Corresponding authors: (E-mail: seemabisla07@gmail.com)

decomposition, polyol, and co-precipitation processes. The co-precipitation method is widely used by researchers because of its special advantages, which include high purity, low cost, uniform doping element distribution, and stoichiometry which requires little preparation time.

The Al_2O_3-doped iron oxide was synthesized in the current work under various physical conditions and concentrations. The primary objective of the present study was to develop novel composite materials with enhanced attributes of both the host and guest materials. The co-precipitation technique was employed to synthesize Al_2O_3-doped α-Fe_2O_3 nanoparticles and thenthe structural, optical, and magnetic properties were studied andresults were discussed in subsequent para's of paper.

2 Sample Formation Method

The authors declared that all chemicals used in study were analytical grade and didn't require additional laboratory refinement for study. Al_2O_3-doped Fe_2O_3 nanoparticles were synthesized by the microwave-treated co-precipitation technique with appropriate concentration of $FeCl_3.6H_2O$ and $Al(NO_3)_3 9H_2O$ were dissolved in 100 ml doubly distilled water employed for this study so that mixture with a mustard colour were obtained. Subsequently, a 14.0 pH ammonia solution was added to the mixture, which caused the pH of the mixture to continuously rise and precipitate were formed at about 9.0 pH and washed with ethanol and deionized water. The resulted precipitate were filtered with help of HOFFMAN paper and the filtered cake was dried by microwave radiation for 15 minutes at 150 °C on two settings and thereafter, calcined further at 600 °C for 2hrs. The calcined samples were crushed in agate mortar and fine powder sample were obtained thenfinely powdered samples were kept as a final product and used for further characterization techniques.

3 Instrumentation

3.1 X-ray Diffraction Analysis (XRD)

The sample was examined for X-ray diffractometer analysis using a "Bruker X-Ray Diffractometer" at Cu-K_α (1.5406nm) at Central Instrumentation Facility (CIF), Lovely Professional University (LPU), Phagwara (Punjab), with a scanning range of two theta values of 10^o and 80^o.

3.2 Fourier Transforms Infrared Spectroscopy (FT-IR)

At the Sophisticated Analytical Instrumentation Facility (SAIF) in Punjab, the "Perkin Elmer Spectrum RX-IFTIR" was used to analyze the infrared properties of the materials in therange 400–4000 cm^{-1}.

3.3 Ultraviolet-Visible (UV-Vis) Spectrometer

At the Central Instrument Research Facility, Amity University Haryana (AUH), the optical characteristics of samples were measured using the R928 PMT detector on the "Cary 100 UV-Vis spectrophotometer (Agilent)" in the wavelength range of 190 to 1100 nm.

3.4 Vibrating Sample Magnetometer (VSM)

VSM characteristics were studied for magnetic measurement (magnetization of material "M" vs. applied magnetic field intensity "H") using a "Vibrating Sample Magnetic "Pilani, Jhunjhunu District, Rajasthan, is located in the Central Electronics Engineering Research Institute (CEERI), a division of the Council of Scientific and Industrial Research (CSIR India), with a temperature of +1.5T.

4 Research Outcome

4.1 Structural Properties

XRD is used to identify nanoparticles and their crystalline enhancement nature by using the co-precipitation process of Al_2O_3-doped Fe_2O_3. Fig. 1 displays the XRD pattern of the nanoparticles. Al_2O_3-doped Fe_2O_3 samples with various aluminiumdopant's 0% (pure), 5%, 10%, and 20% results in a small shift in the most intense peak position relative to the usual 2θ value of the (104) peak (2θ = 33.177°, 33.197°, 33.238°, 33.258°).

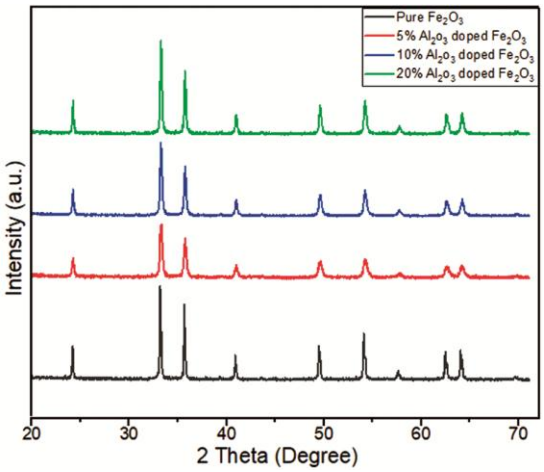

Fig. 1 — shows the XRD spectrum of the material calcined at 600 °C for two hours.

Although, all of these XRD peaks were optimally identified and displayed in the figure according to the rhombohedral unit-cell structure of standard (JCPDS Card No.10-0425)[10]. The increasing intensity of the (104) and (110) orientations can be noticed in these images. This may be because the heating at 600 °C results in increased atom mobility during lattice rearrangement processes. The Al_2O_3-doped Fe_2O_3 nanoparticles' defects could be reduced, and their quality enhanced by the heat energy that was supplied to the atoms *i.e*. decreases in the reflection peaks' of XRD Full Width at Half Maximums (0.375, 0.205, 0.174, 0.143), which reduce as the size of the particle increases (23.087 nm, 42.234 nm, 49.764 nm,60.556 nm).

This is a common size-dependent effect in nanoparticles. Debye-Scherer's equation, which is provided by Eq. (1) was used to compute the mean particle diameter of the Al_2O_3-doped Fe_2O_3 [11].

Eq. (1)

$$G = k\lambda/\beta \cos\theta \quad \ldots(1)$$

Where G, k (k = 0.89), and λ stand for thecrystalline size, shape factorsand wavelength, respectively, β stands for the FWHM (Full Width Half Maxima).

Table 1 tabular data shows that the size of the crystallites increases as the dopant concentration rises. No significant variations were found at the 2θ positions of the most intense peak. However, these changes in lattice constant originate from the difference in ionic radii of Al^{3+} ion 0.535 A˚ and Fe^{3+} ion 0.645A˚ [12,13]. Therefore, it is found that structural lattice parameters decrease as dopant concentration increases.

4.2 FTIR Spectroscopy Study

FTIR analysis was used to identify the functional groups and vibrational bands present in the samples. Fig. 2 shows the IR spectrum of calcined samples. The broad peak observed at wave number 3416 cm^{-1}, 2200 and 1635 cm^{-1} were due to the presence of stretching vibrations of the hydroxyl group (O-H group)[14-18]. The presence of NO_2 and CO_2 in the sample is indicated by the peak location that was detected around, 1376cm^{-1}[19] and might be due to use of ethanol and zinc nitrate during synthesis process.

The sharp peaks found at 610, 614, and 617 cm^{-1} were attributed byO-Fe-O molecules vibrations. Whereas, 533 cm^{-1} were attributed by O-Al-O molecules vibrations respectively[20]. The IR peaks confirmed the synthesis of Al_2O_3 doped Fe_2O_3 nano-crystallines and supports the XRD finding of study.

4.3 Optical Properties

The absorption spectra of Fe_2O_3 nanoparticles doped with Al_2O_3 at 600 °C are displayed in Fig. 3. The spectrum of each sample shows absorption peaks in the wavelength range of 510-590nm.UV-Vis was used to calculate the optical band gap of the samples with various Al_2O_3 dopants as displayed in Fig. 4. The band gap is calculated by the x-axis intercept obtained by drawing a tangent to the curve. Pure Fe_2O_3 nanoparticles have maximum wavelength values that are the same as those of haematite[23]. The optical band gap energy of nanoparticles was calculated using Tauc's relation[24].

Eq. (2)

$$(\alpha h\nu) = A(h\nu - E_g)^n \quad \ldots(2)$$

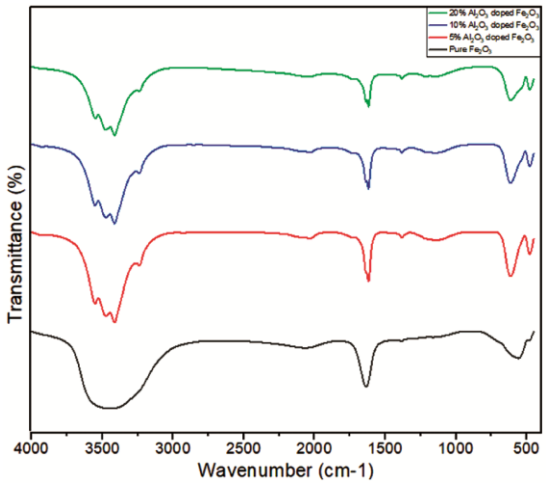

Fig. 2 — shows the IR spectrum of the material calcined at 600 °C for two hours.

Table 1 — Shows the computed grain size of Al_2O_3-doped Fe_2O_3 NPs that were calcined at 600 °C for two hours.

Sr. No.	Dopants Conc. 600°C(2 hours)	Most Intense Peak (2θ)	FWHM(β)	Grain Size(G)
1	Pure	33.177	0.375	23.087
2	5%	33.197	0.205	42.234
3	10%	33.238	0.174	49.764
4	20%	33.258	0.143	60.556

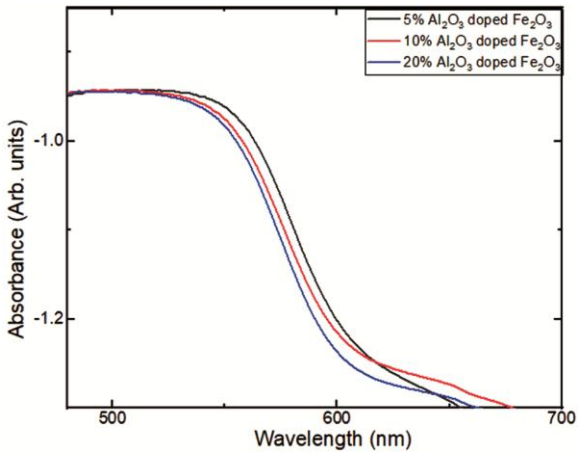

Fig. 3 — shows the UV spectroscopy absorbance graph of the material calcined at 600 °C for two hours.

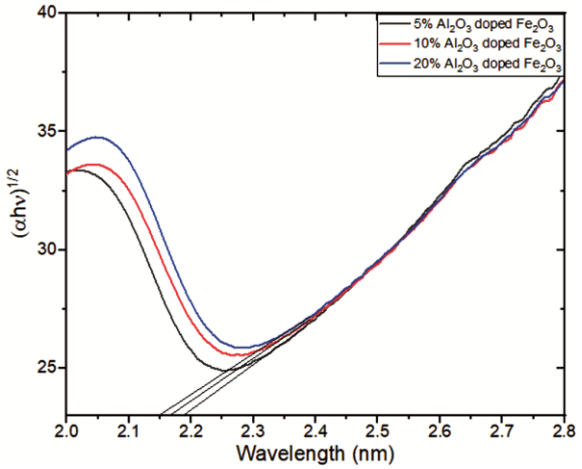

Fig. 4 — shows the UV spectroscopy tauc plot of the material calcined at 600 °C for two hours.

Where α indicates the absorption. In this case, hν represents the incident photon energy of light, A is a constant, and E_g indicates the band gap energy. Depending on the kind of optical transition, n is a constant that changes (n = 2 indirect transitions).

The findings show that when the Al_2O_3 dopant is added, the energy band gap decreases. Moreover, there is a tendency for the wavelength of the λ edge absorption to be greater in size, which suggests a red shift and a reduction in the band gap in the sample[25]. For the samples containing 5%, 10%, and 20% impurities, respectively, the band gap values are 2.19, 2.17, and 2.15eV.

This decrease in band gap reflects that less energy is required to excite charge carriers as concentration increases. Consequently, the difference in ionic radii between the Fe^{3+} ion and the Al^{3+} ion is the cause of these variations in the lattice constant[26]. When the smaller Al^{3+} ion takes the place of the Fe^{3+} ion.

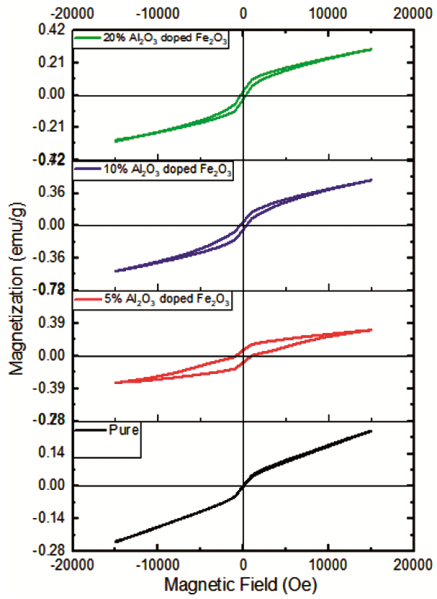

Fig. 5 — shows the vibrating sample magnetometers of the material calcined at 600 °C for two hours.

Table 2 — Shows the computed vibrating sample magnetometers of Al_2O_3-doped Fe_2O_3nanoparticles that were calcined at 600 °C for two hours.

S. No.	Dopant Conc. 600°C 2hour	M_s (emu/g)	M_r (emu/g)	H_c (O_e)	M_r/M_s
1	Pure	23.7×10^{-2}	4.5×10^{-2}	90.55	0.189
2	5%	30.7×10^{-2}	7.2×10^{-2}	875.38	0.234
3	10%	50.6×10^{-2}	4.3×10^{-2}	403.27	0.084
4	20%	29.6×10^{-2}	2.9×10^{-2}	322.20	0.097

4.4 Magnetic Properties

VSM was used to determine the sample'smagnetic properties at room temperature with various Al_2O_3 dopants. In Fig. 5, the hysteresis loops show that the Al_2O_3-doped Fe_2O_3 nanoparticles are ferromagnetic. Table 2 shows that as Al_2O_3 concentration increases, saturation magnetization (M_s) was observed to increase from pure to 10%, but at 20% concentration, M_s decreases. Al_2O_3 doped Fe_2O_3 nanoparticle coercivity (H_c) decreases as the Al_2O_3 concentration rises from 5 to 20%. The Fe_2O_3 nanoparticles doped with 5% Al_2O_3 have the greatest H_c (875.38O_e). It shows that Fe_2O_3 spin canting is properly increased by low levels of Al_2O_3 doping and is progressively impaired by high doping concentrations. The remanence (M_r) of Al_2O_3-doped Fe_2O_3 nanoparticles decreases with an increase in Al_2O_3 the concentration. It reveals that the ferromagnetic strength of Fe_2O_3 nanoparticles is decreasing.

The analysis of the literature report that when the smaller Al^{3+} ion replaces the Fe^{3+} ion[27], the squareness factor (M_r/M_s) in the samples decreases as the Al_2O_3 content rises. The material's single-domain or multi-domain magnetic structure is verified by the squareness factor value. The magnetic structure represents a domain if the squareness factor value is less than 0.5; otherwise, it is analyzed to be a single domain. In this case, the squareness factor values for every sample are less than 0.5, showing that the synthesized sample has a multi-domain magnetic structure[28]. The tabular data emphasized that the 5% alumina doped Fe_2O_3 samples have wide range of applied magnetic field (H_c) intensity and these materials are proving their suitability in formation of core of transformer.

5 Conclusion

The co-precipitation method was used to prepare the Al_2O_3-doped Fe_2O_3 nanoparticles. The XRD reflects that the particle size is increased from 42.23 to 60.55nm. The infrared spectroscopic results concluded that as usual peaks of hydroxyl group vibrations were found in band formation at about 3000 cm^{-1}, 2200 cm^{-1},1635 cm^{-1} and the sharp peaks at 610, 614, and 617 cm^{-1} were attributed by O-Fe-O molecules vibrations whereas, 533 cm^{-1} were attributed by O-Al-O molecules vibrations. The optical band gap were calculated via Tauc plot and the values show inverse trend 2.19 to 2.15 eV. The VSM tools were used to analyze the magnetic characteristics of calcined samplers and the results reveals that saturation magnetization are highest for dopant alumina10% concentration (M_s = 50.6×10^{-2} emu/g) and coercivity were highest for dopant alumina 5% concentration (H_c = $875.38O_e$) respectively among all the calcined samples. The 5% alumina doped Fe_2O_3 samples have wide range of applied magnetic field (H_c) intensity and these materials are proving their suitability in formation of core of transformer.

References

1 Riaz S, Hussain A, Guo Y J, Khaleeq-ur-Rehman M & Naseem S, *Environ Mater Res (ACEM)*, 1 (2016).

2 Madhukara N M, Bhojya N H S, Nagaraju G M, Vinuth K V, Rashmi S K, *Springer Science+Business Media, LLC, part of Springer Nature*, 2018.

3 Chibani A, Kendil D, Benhaoua B, Kemer Chou I & Bekkar D, *J Nanomater Biostruct*, 17 (2022) 1463.

4 Sundhar P R, Krishna H, Gumpu M B, Babu K J, Kulandaisamy A J & Rayappan J B B, *Materials* 16 (2023) 59. https://doi.org/10.3390/ma16010059.

5 Beril K O & Ergun C, *Ceram Int J*, (2015) 411994; https://doi.org/10.1016/j.ceramint.2014.09.103.

6 Chibania A, Kendilb D, Benhaouac B, Kemerchoud I, Bekkare D, *Digest J Nanomater Biostruct*, 17 (2022) 1463.

7 Sergey V, Gudkov Dm E, Burmistrov, Veronika V S, Anastasia A S & Andrey B L, *Nanomater (Basel)*, 12 (2022) 2635.

8 Benamara M, Zahmoul N, Teixeira S S, Graça M P F, El Mir L & Valente M A, *J Electron Mater*, (2022); https://doi.org/10.1007/s11664-022-09539-1.

9 Sergey V G, Dmitriy E B, Veronika V S, Anastasia A S & Andrey B L, *Nanomaterials (Basel)*, 12 (2022) 2635.

10 Jiao W Q, Yue M B., Wang Y M & He M Y, *Microporous Mesoporous Mater*, 147 (2012) 167.

11 Manikandan V, Jayanthi P, Priyadharsan A, Vijayaprathap E, Anbarasan P M & Velmurugan P, *J Photochem Photobiol A Chem*, 371 (2019) 205.

12 Francisca R & Sónia S, *J Compos Sci*, 8 (2024) 33.

13 Rasheed R T, Al-Algawi S D, Kareem H H & Mansoor H S, Rasheed *et al*., *Chem Sci J*, 9 (2018) 4.

14 Farahmandjou M, Khodadadi A & Yaghoubi M, *J Supercond Novel Magnetism*, 33 (2020) 3425.

15 Sigamani S & Dubey R S, *Rom J Inform Sci Technol*, 23 (2020) 105.

16 Singh J, Arun M, Singh K, Khosla R, Kumar S & Gyaneshwar S, *J Mater Sci Mater Electron*, 29 (2017) 3850.

17 Dara P K, Mahadevan R, Digita P A, Visnuvinayagam S, Kmar L R G, Mathew S, Ravishankar C N, Anandan R, *SN Appl Sci*, 2 (2020) 665.

18 Momtaz F, Momtaz E, Mehrgardi M A, Tahmineh M M, Narimani T & Poursina F, *Sci Rep*, 14 (2024) 7356.

19 Beltran J J, Barrero C A & Punnoose A, *Phys Chem Chem Phys*, 17 (2015) 15284.

20 Isokoski K, Poteet C A & Linnartz H, *Astron Astrophys*, 555 (2013) 4.

21 Kumar P, Sharma V, Sing J P, Kumar A, Chahal S, Sachdev K, Chae K H, Kumar A, Asokand K & Kanjilal D, *J Magn Magn Mater*, 489 (2019) 165398.

22 Singh S, Hitkari G & Pandey G, *Inorg Nano-Metal Chem*, (2019) 157151.

23 Kabir F, Murtaza A, Saeed A, Ghani A, Ali A, Khan S, Kaili Li, Zhao Q, Yao K K, Zhang Y & Yang S, *Ceram Int*, (2022) https://doi.org/10.1016/j.ceramint.(2022).03.096.

24 Joseph J A, Sinitha B N, Sarah J S, Stephen K R, Sadasivan S & Rachel R P, *J Appl Electrochem*, 51 (2021) 521.

25 Deotale A J & Nandedkar R V, *Direct Mater Today*, 3 (2016) 2069.

26 Farahmandjou M & Khodadadi A & Yaghoubi M, *J Supercond Novel Magn*

27 https://doi.org/10.1007/s10948-020-05569-0.

28 Sharmin M & Podder J, *Semicond Sci Technol*, 34 (2019) 075033.

29 Luo H, Rai B K, Mishra S R, Nguyen V V & Liu J P, *J Magnet Magn Mater*, 324 (2012) 2602.

30 Sharma R, Hooda N, Hooda A & Khasa S, *J Alloys Compd*, 965 (2023) 171394.